ARTICLE

Dynamic Magnetic Fields Remote Control Apoptosis *via* Nanoparticle Rotation

Enming Zhang,[†,⊗,*] Moritz F. Kircher,[‡,§,⊥,⊗] Martin Koch,[∥] Lena Eliasson,[†] S. Nahum Goldberg,[#,▽] and Erik Renström[†,*]

[†]Department of Clinical Sciences Malmö, Lund University, Malmö 205 02, Sweden, [‡]Department of Radiology, Memorial Sloan-Kettering Cancer Center, New York, New York 10065, United States, [§]Department of Radiology, Weill Cornell Medical College, New York, New York 10038, United States, [⊥]Center for Molecular Imaging and Nanotechnology, Memorial Sloan-Kettering Cancer Center, New York, New York 10065, United States, [∥]Stetter Elektronik, Seeheim-Jugenheim, Hessen 64342, Germany, [#]Laboratory for Minimally Invasive Tumor Therapies, Department of Radiology, Beth Israel Deaconess Medical Center/Harvard Medical School, Boston, Massachusetts 02215, United States, and [▽]Division of Image-guided Therapy and Interventional Oncology, Department of Radiology, Hadassah Hebrew University Medical Center, Jerusalem, Israel. [⊗]These authors contributed equally to this work.

ABSTRACT The ability to control the movement of nanoparticles remotely and with high precision would have far-reaching implications in many areas of nanotechnology. We have designed a unique dynamic magnetic field (DMF) generator that can induce rotational movements of superparamagnetic iron oxide nanoparticles (SPIONs). We examined whether the rotational nanoparticle movement could be used for remote induction of cell death by injuring lysosomal membrane structures. We further hypothesized that the shear forces created by the generation of oscillatory torques (incomplete rotation) of SPIONs bound to lysosomal membranes would cause membrane permeabilization, lead to extravasation of lysosomal contents into the cytoplasm, and induce apoptosis. To this end, we covalently conjugated SPIONs with antibodies targeting the lysosomal protein marker LAMP1 (LAMP1-SPION). Remote activation of slow rotation of LAMP1-SPIONs significantly improved the efficacy of cellular internalization of the nanoparticles. LAMP1-SPIONs then preferentially accumulated along the membrane in lysosomes in both rat insulinoma tumor cells and human pancreatic beta cells due to binding of LAMP1-SPIONs to endogenous LAMP1. Further activation of torques by the LAMP1-SPIONs bound to lysosomes resulted in rapid decrease in size and number of lysosomes, attributable to tearing of the lysosomal membrane by the shear force of the rotationally activated LAMP1-SPIONs. This remote activation resulted in an increased expression of early and late apoptotic markers and impaired cell growth. Our findings suggest that DMF treatment of lysosome-targeted nanoparticles offers a noninvasive tool to induce apoptosis remotely and could serve as an important platform technology for a wide range of biomedical applications.

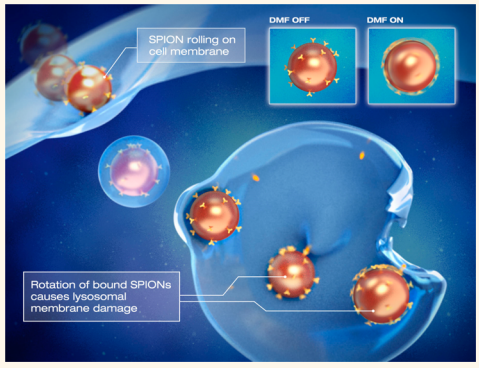

KEYWORDS: dynamic magnetic field · nanoparticle rotation · iron oxide · magnetic nanoparticles · lysosomes · antibody · LAMP1 · permeabilization · apoptosis

Superparamagnetic iron oxide nanoparticles have found widespread applications in the biomedical field spanning *in vitro* diagnostic tests such as nanosensors,[1−4] *in vivo* imaging[5−9] and therapies such as magnetic fluid hyperthermia[10,11] or drug delivery.[12,13] Recent investigations have also explored the capability of controlling the position or temperature of magnetic nanoparticles within cells and tissues by remote application of magnetic fields. So far, this has been investigated using permanent magnets that set nanoparticles in a longitudinal motion, using alternating magnetic fields, or through rotating permanent magnets outside of the tissues of interest.[14,15] In the latter scenario, the nanoparticles describe circular motions but do not individually rotate around their own axis. The combination of alternating magnetic fields and magnetic nanoparticles allows one to transform energy into forces or heat.[16,17] Hyperthermia is used as an adjunctive treatment in cancer therapy; here, high-frequency alternating (but not moving) magnetic fields in the kilo- to megahertz (kHz−MHz) range have been used to kill cancer cells loaded with magnetic

* Address correspondence to erik.renstrom@med.lu.se, enming.zhang@med.lu.se.

Received for review December 9, 2013 and accepted March 5, 2014.

Published online 10.1021/nn406302j

nanoparticles through thermal induction.[18−20] However, such treatment is not without risks, particularly near thermally sensitive structures such as the gut or gallbladder if nanoparticles are injected systemically, as the heat induction cannot be controlled spatially with high precision and could cause tissue necrosis. Therefore, in contrast to thermal ablation systems, ambient temperature increases >46 °C are not desirable for purposes of remote controlling apoptosis with magnetic fields.[21]

Fundamentally different from prior studies using high frequency alternating magnetic fields that cause apoptosis *via* heat induction, we describe here a principle of controlling nanoparticle rotation and inducing apoptosis *via* mechanical forces exerted on membranes by targeted nanoparticles. Specifically, we have developed a device that enables us to induce and precisely control the rotation of magnetic nanoparticles around their own axis, termed here 'dynamic magnetic field (DMF) generator'. The DMF generator creates a dynamic force field, which is converted inside the particle into a magnetic flux field *B*, which operates on a SPION particle with a magnetic Moment *M* and a moment of inertia *I*. The field generates a torque $\vec{\tau}$ equal to $\vec{\tau} = \vec{\mu} \times \vec{B}$. This enables for the first time to induce rotation of individual magnetic nanoparticles around their own axis, and allows precise control of the rotation speed.

We demonstrate that induction of this kind of rotation in targeted superparamagnetic iron oxide nanoparticles (SPIONs) can be used to remotely activate apoptosis. We show that SPIONs conjugated with LAMP1 (Lysosomal-associated membrane protein 1) antibodies (LAMP1-SPION)[22] internalize into cells and bind to lysosomal membranes. We observed that subsequent remote activation of the dynamic magnetic field causes mechanical disruption of lysosomes, which leads to apoptosis *via* extravasation of lysosomal contents into the cytoplasm and a decrease of intracellular pH. While the unique ability of rotational control of nanoparticles is demonstrated here in a specific biological application, the same principle should enable many other new applications in the fields of nanotechnology and nanomedicine.

RESULTS

Dynamic Magnetic Field Stimulation Results in Rotation of Individual Nanoparticles. A DMF generator was developed to control directional movement and self-centered rolling (Figure 1A). To demonstrate the pattern of the particle movement, we first monitored the rotation of larger magnetic beads of different sizes (5.8, 1, 0.5, and 0.3 μm diameter) by filming them in a cell culture dish under a microscope. Once the DMF is switched on, the beads start to rotate around their own axis, which also causes a slow directional movement of the beads across the floor of the dish (Figure 2 and Supporting Information Movies 1 and 2). This clearly demonstrated that the applied DMF treatment enables a self-turning of magnetic particles. The speed of rotation can be controlled by varying the frequency setting on the DMF device (illustrated in Supporting Information Movie 1 and 2). This observation suggested that the DMF could be used to contrive a virus-like interaction between the SPIONs and the cell surface, which in turn could enhance internalization of the SPIONs into the cytosol. Once the SPIONs have internalized into the intracellular compartments, *e.g.*, endosomes or lysosomes, the loaded SPIONs can be operated noninvasively by DMF to regulate the cellular compartmental activities and further cell functions (Figure 1B).

Dynamic Magnetic Field Stimulation Enhances Uptake of Superparamagnetic Nanoparticles. Internalization of SPIONs into living cells was reported previously.[23−25] We first evaluated the internalization efficiency in the absence or presence of DMF stimulation. To monitor the process of SPION internalization, we used fluorescently labeled (TRITC) 100-nm SPIONs and incubated them with rat insulinoma cells (INS-1). We also tested 300-nm SPIONs, but these exhibited markedly lower loading efficiency. We then applied a DMF field for 20 min at a frequency of 20 Hz, before staining the cells using the plasma membrane marker CellMask, the lysosomal marker LysoTracker Green, and the nuclear marker Hoechst 34580. The cells were then imaged by live confocal microscopy, which demonstrated that the majority of the SPIONs were loaded into the lysosomes after 20 min of DMF treatment (Figure 3A). A total of 71.2 ± 3.8% of SPIONs colocalized with the lysosomal marker LysoTracker Green, while only 18.2 ± 2.2% of SPIONs colocalized with the plasma membrane and early endosome probe CellMask (Figure 3B). Conversely, 91 ± 8.7% of the LysoTracker Green fluorescence appeared in conjunction with SPIONs, which means that nearly all lysosomes contained several loaded SPIONs (Figure 3C). Next we conjugated SPIONs with an antibody against the lysosomal membrane protein, LAMP1 (LAMP1-SPION). We compared the loading efficiencies between SPION and LAMP1-SPION, in order to evaluate if the conjugation of the LAMP1 antibody enhanced internalization and loading into the lysosomes. LAMP1-SPION nanoparticles were more efficiently loaded into the lysosomes than the unconjugated SPIONs, and the loading efficiency after 20 min. DMF treatment averaged 13.3 ± 2.3% and 21.2 ± 2.4% for SPIONs and LAMP1-SPIONs, respectively (Figure 3D).

Dynamic Magnetic Field Stimulation Can Injure Lysosomes *via* Antibody-Conjugated Superparamagnetic Nanoparticles. To evaluate whether DMF treatment has the potential to injure lysosomes in LAMP1-SPION-loaded cells, we visualized the lysosome compartment with the marker LysoTracker Green. After DMF-facilitated loading of the LAMP1-SPION nanoparticles, the cells were cultured at

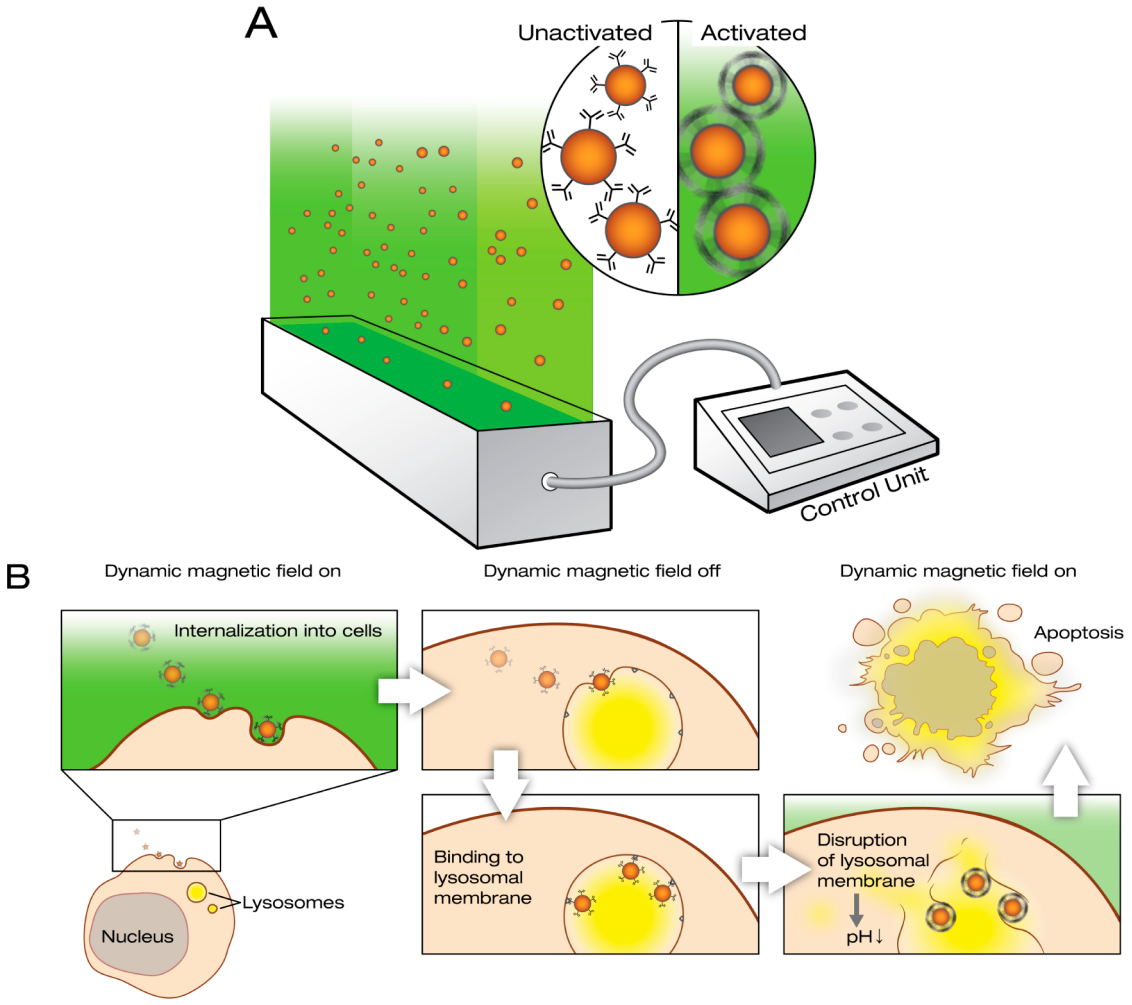

Figure 1. DMF controls rotation of magnetic nanoparticles. (A) Schematic representation of the DMF generator. The device controls rotation and movement of magnetic nanoparticles (SPIONs) with a low frequency (10−40 Hz) field. In contrast to reported alternating magnetic field generators, the DMF generator causes the nanoparticles to rotate around their own axis. (B) Principle of use of the DMF generator: remote induction of apoptosis. When targeted nanoparticles (LAMP1-SPIONs) first come into contact with cell membranes, their internalization can be enhanced by activation of slow nanoparticle rotation. This causes rotational motion (rolling) of the nanoparticles across the cell membrane and eventually internalization. Once internalized, the LAMP1-SPIONs enter lysosomes and bind to the lysosomal membrane. When the DMF is activated at this point, the nanoparticles start to rotate and the resulting shear forces cause injury to the lysosomal membrane. This in turn causes leakage of the lysosomal contents into the cytoplasm, leading to a decrease in its pH and subsequently apoptosis.

37 °C for 40 min to allow binding of the antibody paratope on the nanoparticles to LAMP1 in the lysosomal membrane. After that culture period, any remaining LAMP1-SPION nanoparticles outside the cells were removed by washing, before subjecting the cells to DMF treatment (20 Hz) for 20 min. The capability of the DMF treatment to disrupt the compartments of the lysosomes was evaluated by assessing changes in LysoTracker Green fluorescence intensity. Indeed, in LAMP1-SPION-loaded cells, the DMF treatment significantly decreased LysoTracker Green fluorescence by 75% as compared to cells loaded with conventional SPIONs without the LAMP1 antibody (483.6 ± 84.2 *vs* 120.3 ± 20.9 AU for SPION- and LAMP1-SPION-treated cells, respectively (Figure 4A,B). A dynamic depiction of this finding is shown in Supporting Information Movie 3 (green = LysoTracker Green; red = LAMP1-SPIONs). To confirm these findings, we next used the acidotropic probe (pK_a = 5.2) LysoSensor Green DND 189.[26] The rationale for this experiment was that disruption of lysosomes would reduce the volume of the very acidic compartments in the cell and lead to a decrease in LysoSensor Green fluorescence (Figure 4C and 4D). Prior to DMF treatment, we found no difference in fluorescence intensity between SPION- and LAMP1-SPION-loaded cells. DMF treatment had no effect in SPION-loaded cells. In contrast, in LAMP1-SPION-treated cells, fluorescence intensity dropped (769.5 ± 82.5 *vs* 368.4 ± 69.6 AU/cell in SPION- *vs* LAMP1-SPION treated cells, respectively; $P < 0.001$). While the induction of heat—in contrast to high frequency alternating magnetic fields—was not expected *a priori* given the low frequency of our dynamic magnetic fields, we excluded this possibility by monitoring temperature

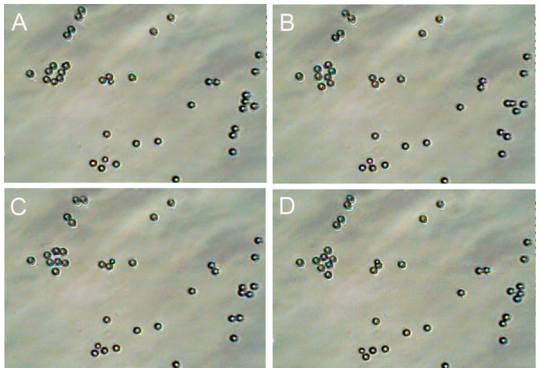

Figure 2. Illustration of DMF-induced rotation of magnetic particles. To enable better visualization of the effect of the DMF on magnetic particles under the microscope, larger micrometer sized magnetic beads (diameter 5.8 μm) were used. A dish containing beads in a physiologic salt solution (Krebs buffer) was placed in the vicinity of the DMF device. Once the DMF is switched on, the beads start to rotate around their own axis, which also causes a slow directional movement of the beads across the floor of the dish. The beads complete a rotation of 360° in seconds (time depends on the viscosity of the liquid) between the images A and D. The speed of rotation can be controlled by varying the frequency setting on the DMF device and in this experiment was varied between 5 and 15 Hz. This can be better appreciated in the accompanying Supporting Information Movie 1.

runs in phantoms. These experiments showed that no significant change in temperature was caused by the DMF induced magnetic field (Figure 5). Taken together, these results suggest that the remote application of the DMF treatment causes permeabilization of lysosomal compartments, induced *via* the torque of the membrane-bound LAMP1-SPIONs.

Effects of Dynamic Magnetic Field Stimulation of Superparamagnetic Nanoparticles in Human Primary Cells. To monitor the LAMP1-SPION loaded lysosomes, we coated SPIONs covalently with both LAMP1 antibodies and the fluorescence marker TRITC (TRITC-LAMP1-SPION). To further validate the possibility to translate our findings to clinical settings, we used isolated primary cells from human pancreatic islets and seeded on glass bottom Petri dishes. Then, TRITC-LAMP1-SPIONs were added to cell culture medium, followed by DMF treatment or no treatment, and finally, the cells were fixed for confocal microscopy. Human primary islet cells contained larger lysosomes than INS-1 cells as assessed by TRITC fluorescence (Figure 6A, upper). To assess colocalization of LAMP1 and TRITC-LAMP1-SPION, LAMP1 was detected by indirect immunocytochemistry using a Cy2-tagged secondary antibody. In cells not exposed to DMF treatment, LAMP1 and TRITC-LAMP1-SPION colocalized by 49.9 ± 9.2%, which was not significantly affected by DMF treatment (54.8 ± 9.5%) (data not shown). These results indicate that the bonds between LAMP1 and TRITC remain stable during DMF treatment. Interestingly, the TRITC-LAMP1-SPIONs loaded into the cells mainly appeared around the boundaries of structures, which are likely to represent a location in

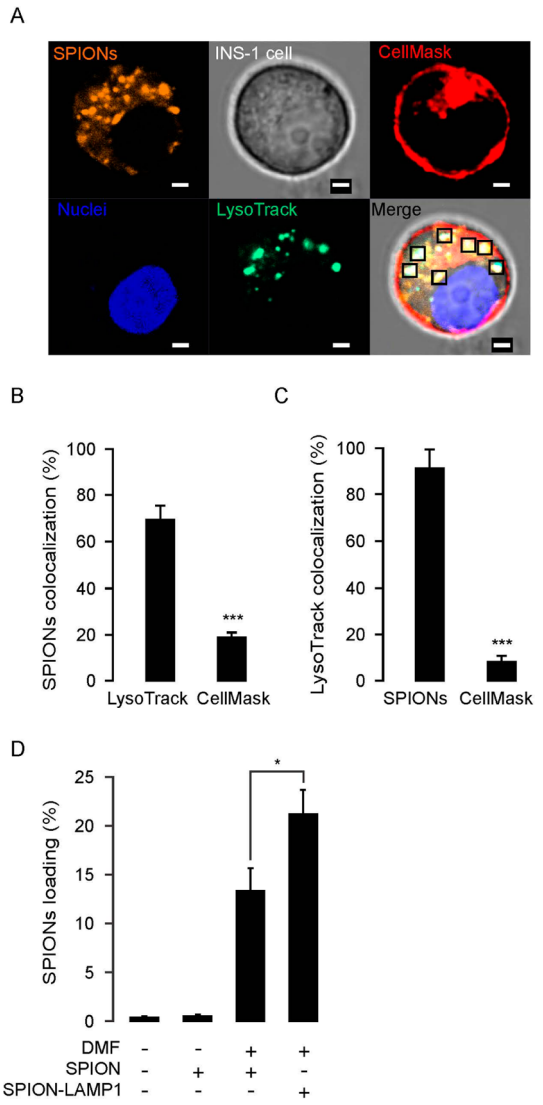

Figure 3. Loading of magnetic nanoparticle into lysosomes in INS-1 cells. (A) Confocal imaging of SPIONs location in INS-1 cells. The SPIONs conjugated with the fluorescent dye TRITC (orange) were incubated with living cells in a static magnetic field for 5 min. Thereafter, the cells were treated by DMF with 20 Hz, for 20 min, and then confocal microscopy images were obtained. Plasma membrane and early endosomes were stained with CellMask (red); nuclei and lysosomes were stained with Hoechst 32580 (blue) and LysoTracker Green (green), respectively. The squares in the merge stack indicate SPIONs located in the lysosomes. Scale bars = 2 μm. (B) Statistical analysis of SPION colocalization with LysoTracker Green and CellMask under same conditions as in (A). (C) Colocalization analysis of lysosomes with SPION and CellMask under same conditions as (A). (D) Loading efficiency of LAMP1 antibody conjugated SPIONs (LAMP1-SPION) increased under condition with the DMF treatment. The loading efficiency is calculated by the ratio of TRITC fluorescence intensity (yellow) over nuclear intensity. The data was collected from three independent experiments. *$p < 0.05$ and ***$p < 0.001$.

the lysosomal membrane (Figure 6B). However, after a second round of DMF treatment, most of the LAMP1 was apparently separated from the TRITC-LAMP1-SPIONs (Figure 6A, bottom) and the SPIONs aggregated tightly (Figure 6C). DMF treatment also led to

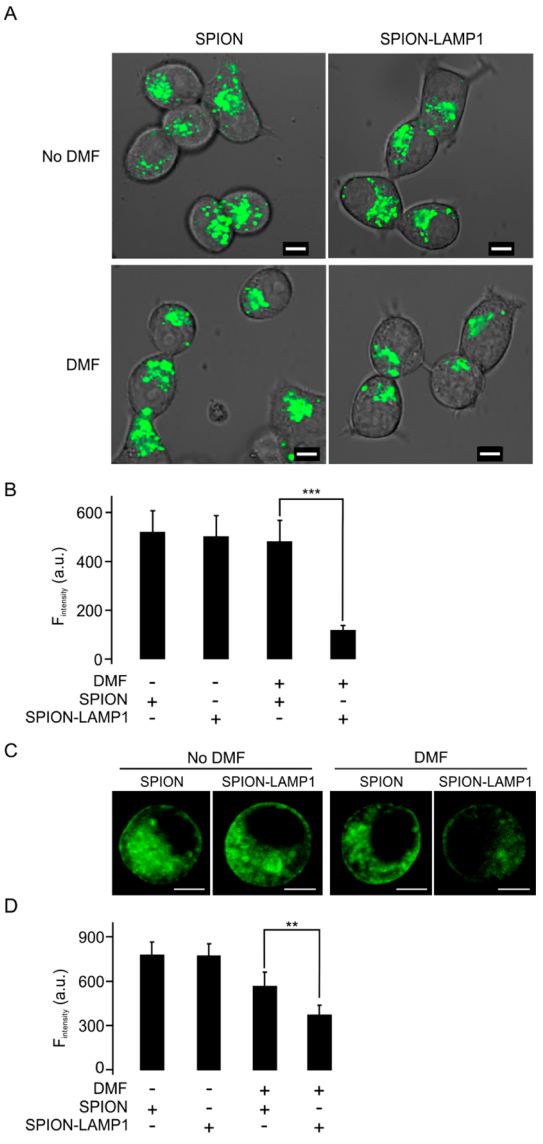

Figure 4. DMF treatment decreases intracellular lysosomes and the pH in LAMP1-SPION loaded INS-1 cells. (A) The cells were treated by DMF (20 Hz, 20 min) and lysosomes stained with LysoTracker Green. Scale bars = 5 μm. (B) Mean intensity of fluorescence was measured under the different conditions in (A). (C) Representative confocal images indicate the intracellular pH value using an acidotropic probe, LysoSensor Green DND 189 in INS-1 cells. Scale bars = 5 μm. (D) Mean fluorescence intensities were measured as in (C). Data collected from five experiments with at least 6 cells under each condition. **$p < 0.01$, ***$p < 0.001$.

a marked downward shift in the distribution of lysosomal sizes (Figure 6D), and accordingly, the average size of lysosomes decreased from 1.77 $\pm$ 0.06 μm (n = 141) to 0.79 $\pm$ 0.05 μm (n = 105) after DMF treatment (Figure 6E). These results suggest that the second round of DMF treatment in cells loaded with TRITC-LAMP1-SPIONs results in a certain degree of damage to the lysosome membrane. However, a potential alternative explanation could be that the detachment of TRITC-LAMP1-SPIONs occurs from the lysosome membrane without disruption which can lead to the particles aggregating in the center of the still intact lysosomes. To address this possibility, the subcellular locations of the LAMP1-SPIONs were further identified by transmission electrical microscopy (TEM). The TEM images clearly showed that LAMP1-SPION particles had accumulated within intracellular compartments after loading into cells (Figure 6F, left). In contrast, after the second round of DMF treatment, the LAMP1-SPIONs were scattered throughout the cells (Figure 6F, right). These results demonstrate that DMF-induced rotational movement of LAMP1-SPIONs is also capable of disrupting lysosomal membranes in human primary cells.

Consequences of DMF-Mediated Disruption of Lysosomes. Disruption of lysosomes has previously been reported to activate apoptotic reactions.[27] To determine whether DMF treatment can elicit apoptosis in LAMP1-SPION-loaded cells, we measured the extent of apoptosis in INS-1 cells with and without DMF. Annexin V and 7-AAD were used to indicate early and late stage apoptosis, respectively (Figure 7A). After DMF treatment, early and late apoptosis in LAMP1-SPION loaded INS-1 cells significantly increased from 4.56 $\pm$ 0.55% to 12.45 $\pm$ 1.6% and from 0.73 $\pm$ 0.17% to 1.31 $\pm$ 0.16%, as evidenced by positive staining for Annexin V or 7-AAD, respectively (Figure 7B and 7C). Furthermore, the elevated rates of apoptosis also had consequences on cell proliferation during culture. A single 20 min. DMF treatment (20 Hz) in SPION-loaded cells had no significant effect on cell number during a 6-days culture period when compared to control cells. In contrast, the number of LAMP1-SPION loaded cells after DMF treatment was significantly ($p < 0.001$) lower from day 2 and onward (Figure 7D). These results suggest that the attack on lysosomes *via* DMF-activated lysosomal membrane-targeted SPIONs prompts apoptotic cell death and affects the growth of the cell population.

DISCUSSION

Here we described a novel biomedical platform based on a unique dynamic magnetic field generator, which in combination with superparamagnetic nanoparticles can be utilized for various new applications.

Several prior studies have investigated the effect of 'alternating magnetic fields' on magnetic nanoparticles.[14,15,18,28−31] These studies generally used high-frequency (kHz range) alternations in the magnetic field polarity, and observed that targeted iron oxide nanoparticles caused damage to cellular membranes leading to permeabilization. Energy dissipated locally as heat by the iron oxide nanoparticles was thought to lead to disruption of lipid bilayers. Huang *et al.*[32] demonstrated a temperature-induced change in fluorescence when a fluorochrome was attached to a magnetic nanoparticle and exposed to an alternating magnetic field, whereas no change was observed in free fluorochromes.

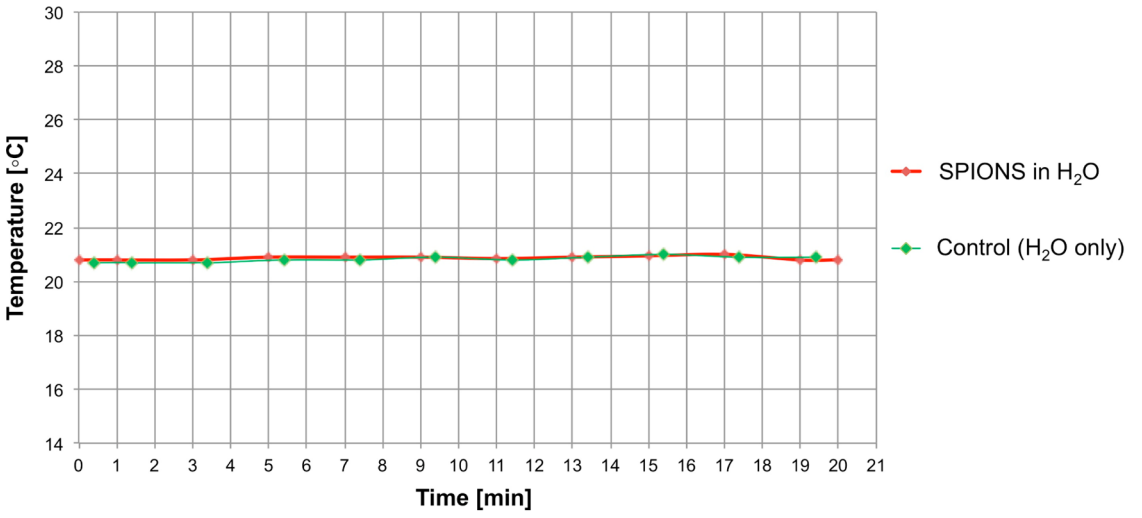

Figure 5. DMF-field induced SPION rotation does not increase temperature. A dish with 100 nm SPIONs (10 mg/mL) in water and a control dish containing water only, each containing a temperature probe, were placed simultaneously on the DMF device. The dishes were then subjected to the DMF field for 20 min at 20 Hz. No significant change in temperature was observed in either the dish with the SPIONs (red curve) or the control dish (green curve).

In contrast to these reports using high-frequency alternating (but not dynamic) magnetic fields, our DMF approach uses low-frequency (~10−20 Hz), dynamic (*i.e.*, moving) magnetic fields of ~30 mT that uniquely induce rotation of every individual particle in the field around their own axis (Figure 1, Supporting Information Movies 1 and 2). The speed of this rotation (and its direction) can be controlled by varying the frequency setting on the device. For example, at lower frequencies nanoparticles can be prompted to roll over cell membranes, which may mimic the movement of viruses along cell membrane surfaces[33] and increase the efficiency with which nanoparticles internalize into cells. Higher rotational speeds can be used in order to destroy particular targets *via* rotational shear forces without inducing unwanted thermal effects. Molecular simulations of lipid bilayers have shown that both incremental shear and tension can destabilize cell membranes, and that the energy that is required to cause such membrane damage can be achieved with rotating magnetic nanoparticles.[15,34] We have applied the DMF on LAMP1 antibody-conjugated superparamagnetic iron oxide nanoparticles to facilitate nanoparticle uptake into cells and to disrupt the lysosomal membrane as a means to induce cell apoptosis. The DMF approach has two major advantages: (1) nanoparticles can be rotated around their own axis, and (2) no significant heat is created. Heat creation is the presumed mechanism of how high-frequency alternating magnetic fields cause damage to cell membranes.[31] This, however, can potentially cause extensive and unspecific cellular necrosis. By contrast, our DMF technology does not induce heating above the physiological temperature range. By our method, apoptosis can be specifically induced in nanoparticle-loaded cells only and apoptotic cells are removed *in vivo* by endogenous scavenger systems, *e.g*, the innate immune system and macrophages. Tissue damage is thus limited to only the targeted cells, in contrast to procedures leading to supraphysiological temperatures and resultant necrosis, potentially sparing widespread acute inflammatory reactions.

To achieve a high degree of specificity of nanoparticle-mediated intervention, targeting of the nanoparticles to the right cell type and into the desired subcellular compartment is important. Our technology platform represents an example of unique utilization of DMFs to target magnetic nanoparticles to specific intracellular compartments. Previous reports have demonstrated the usefulness of magnetic nanoparticles for controlling activity of plasma membrane receptors or ion channels.[28,29,35] Upon protracted stimulation of receptors or ion channels, there is solid evidence for down-regulation of their activities. One important mechanism of such desensitization is internalization of receptors or ion channels to intracellular sites where they reside in an inactive standby pool. In the context of nanoparticle-mediated activation of receptors or ion channels this means that after activation, the number of the receptors/ion channels in plasma membrane decreases and the desired cellular signals and responses are blunted. Moreover, the magnetic nanoparticles themselves are internalized already after short incubation with live cells *via* the endocytotic pathway.[36,37] We have made use of this property of internalization and facilitated the process by DMF treatment to accelerate delivery of LAMP1 antibody-coated nanoparticles to intracellular compartments. Following down the endocytotic pathway, the LAMP1-SPIONs enter the early- and late-endosomes and afterward they should enter other compartments, *e.g.*, ER, *via* recycling endosomes, or being removed

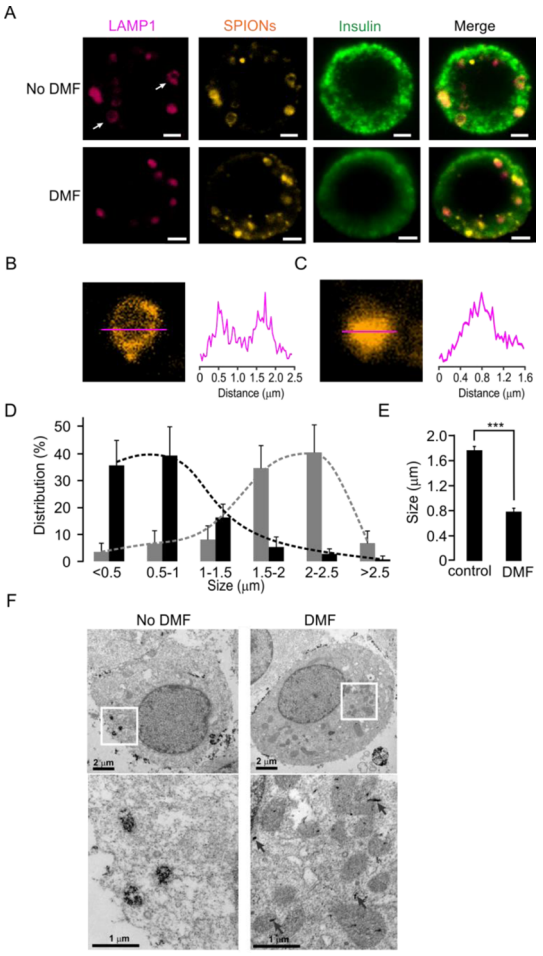

Figure 6. DMF treatment disrupts lysosomes in human pancreatic beta cells after loading with LAMP1-SPIONs. (A) Immunostaining of human islet beta cells with or without DMF treatment. Lysosomes were stained with the anti-LAMP1 antibody (red), SPIONs with TRITC (orange), and islet beta cells with an anti-insulin antibody (green), respectively. Scale bars = 2 μm. (B) The SPIONs are located in the membrane of a lysosome. The intensity profile (right) was derived along the red line in the image (left). (C) Same as (B), except after treatment with DMF. (D) Differences in size distribution of lysosomes before (gray bars) and after (black bars) DMF treatment. (E) Average size of lysosomes without and with DMF treatment. ***$p < 0.001$. (F) Transmission electron microscopy (TEM) images of the intracellular distribution of SPIONs in INS-1 cells. Images on the bottom are magnified versions of the areas indicated with white boxes. While without DMF treatment the LAMP1-SPIONs are clustered in vesicular structures, their distribution is scattered throughout the cytosol after DMF treatment.

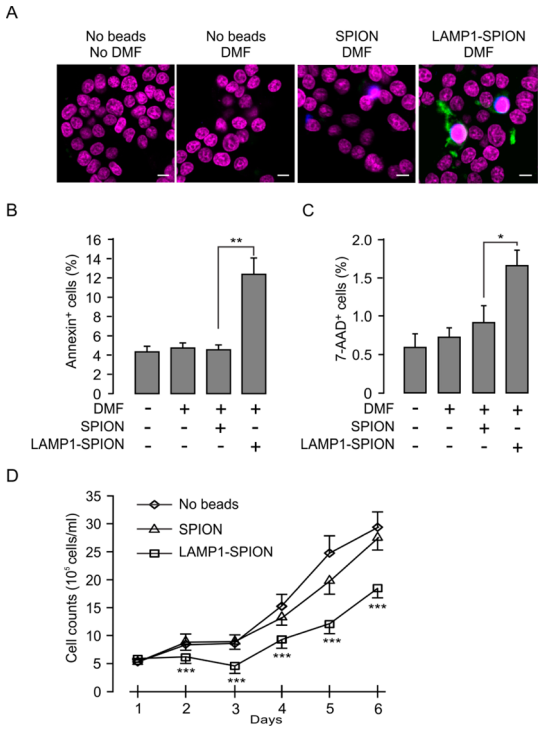

Figure 7. DMF treatment-induced apoptosis in LAMP1-SPION loaded cells. (A) The INS-1 cells were treated with DMF for 20 min at 20 Hz and stained with the nuclear marker Hoechst (purple), the apoptosis marker annexin V (green), and 7-AAD (blue). Scale bars = 5 μm. After 6 h of incubation (5% CO_2, 37 °C), early (B) and late (C) stage apoptosis were detected by percentage of number of annexin V and 7-AAD positive cells to the number of Hoechst stained cells. Note that DMF caused significant increase in apoptosis in LAMP1-SPION-loaded cells compared to when loading was done using conventional SPIONs. Each treatment was conducted with 28 cells. *$p < 0.05$. (D) Decrease of the rate of cell growth in LAMP1-SPION loaded INS-1 cells. Cells were treated with DMF (20 Hz, 20 min.) once/day. Data are from 3 independent experiments and represent mean values ± S.E.M. ***$p < 0.001$.

from the lysosomes,[38] In the lysosomes, the LAMP1 antibody conjugated to the SPION recognizes LAMP1 that is highly expressed in the lysosomal membrane. In response to a low frequency DMF, the now bound SPION generates dynamic forces strong enough to tear the lysosomal membrane, leading to destruction of the lysosome integrity, leakage of lysosomal enzymes and finally induction of apoptosis. In INS-1 cells, we observed that the SPIONs mostly loaded into lysosomes after 20 min DMF treatment (Figure 3A). This preferential lysosomal localization was also observed when SPIONs were located into primary human pancreatic islet cells (Figure 6A). However, as the direction and extent of intracellular membrane trafficking may differ markedly between cell types, the lysosome loading efficiency needs to be carefully evaluated when adopting this application to other cell types. Thus, we envisage that this technology will ultimately provide an avenue for development of tools to regulate specific subcellular compartmental functions including not only the nuclei, but also compartments such as the ER, Golgi apparatus, and different types of endosomes along the intracellular membrane trafficking system. Further studies will be needed to translate our approach *in vivo*. Certain challenges such as the precise delivery of the nanoparticles in a more complex *in vivo* scenario and the application of DMF fields in larger animals and humans in deep organs will have to be overcome. However, ultimate clinical translation using our low frequency DMF approach may be more straightforward than using high-frequency alternating fields, because the DMF fields are not expected to cause nonspecific

heating of tissues through induced eddy currents[31] and should therefore have a better safety profile.

The achievement of rotational control on nanoparticles with the DMF method has many other potential applications beyond the model systems used here, in both biomedical and nonbiological nanotechnology fields. For example, magnetic actuation has been shown to control timing and drug release from vesicles containing iron oxide nanoparticles.[39] The increase in permeability of lysosomal membranes not only can be used to promote apoptosis, such as through the release of proteolytic enzymes and increase in reactive oxygen species, but can also increase the efficacy of drugs trapped in lysosomes. Because sequestration of drugs in lysosomes is responsible for up to 40% of whole tissue drug uptake,[40] lysosomal drug trapping plays an important role in the development of tumor drug resistance.[41] Therefore, with further development, DMF-mediated lysosomal membrane permeabilization could be used to treat cancer drug resistance.

CONCLUSIONS

In summary, using a unique dynamic magnetic field (DMF) generator, we can control rotational movements of superparamagnetic iron oxide nanoparticles (SPIONs) in solution. This rotational nanoparticle movement was applied for remote induction of cell death by injuring lysosomal membrane structures. We covalently coated SPIONs with antibodies targeting the lysosomal protein marker LAMP1 (LAMP1-SPION). Remote activation of slow rotation of LAMP1-SPIONs with 20 Hz for 20 min significantly improved the efficacy of cellular internalization of the nanoparticles. A total of 71.2 ± 3.8% of LAMP1-SPIONs accumulated along the membrane in lysosomes in rat insulinoma tumor cells due to binding of LAMP1-SPIONs to endogenous LAMP1. Further activation of torques by the LAMP1-SPIONs bound to lysosomes resulted in rapid decrease in size and number of lysosomes, attributable to tearing of the lysosomal membrane by the shear force of the rotationally activated LAMP1-SPIONs. This remote activation resulted in increased cell apoptosis and impaired cell growth. Our findings suggest that DMF treatment of lysosome-targeted nanoparticles offers a noninvasive tool to induce apoptosis remotely and could serve as an important platform technology for a wide range of biomedical applications.

METHODS

Nanoparticle Assembly. The protocol of conjugation of LAMP1 antibodies to magnetic nanoparticles was described previously.[22] Briefly, SPION nanoparticles (Micromod, Germany) were amino-functionalized and the density of amino groups per milligram of particles was determined. After washing, the other parts of amino groups were reacted with sulfo-SMCC in PBS-EDTA buffer to introduce maleimide groups on the particle surface. The monoclonal LAMP1 antibody (Abcam, U.K.) was purified with a G-25 column containing PBS/EDTA buffer to remove the glycerin and sodium azide. After purification, the LAMP1 antibody was treated with imnothiolane solution to introduce the SH groups. After the SH-modified antibody was washed with PBS-EDTA buffer in a G-25 column, the maleimide-modified particles were added. The particles were shaken for 1 h at room temperature. Then, cystein was added to quench the remaining reactive sites. Finally, the particles were purified with PBS buffer in magnetic columns in a high gradient magnetic field.

DMF Device. The dynamic fields to control SPION rotation used in this study were created with a DMF generator (DM-01, Feldkraft and Stetter Elektronik, Germany). The device consists of an array of multiphase coil systems, where the coils are displaced against each other. The field can be altered in a highly dynamic fashion. A device-integrated digital controller regulates the frequency as well as the magnetic flux. The dynamic flux produces an electromagnetic gradient force $\vec{F} = (M\nabla)\vec{B}$, where **M** is the magnetic moments of the beads in total and **B** is the dynamic flux density field vector. This vector is established by the **H** field of our device. The magnetic field strength generated by the DMF device used in this study is approximately as large as 30 mT (rms).

Live Cell Imaging. Cells were seeded onto glass coverslips. After DMF treatment, live images were acquired using a Zeiss 510 Meta confocal system with a ×40 water immersion objective (NA =1.2). SPION-TRITC was visualized by excitation at 543 nm and emitted light was collected using a long-pass 560 nm filter. The pinhole was ~1 airy unit and the scanning frame was 512 × 512 pixels. The cellular location of SPION was stained with the plasma membrane marker CellMask (Invitrogen), lysosome marker LysoTracker Green (Invitrogen) and a marker for cell nuclei, Hoechst 34580 (Invitrogen). Image analysis was performed with ZEN 2009 software (Zeiss, Germany). Colocalization was analyzed by a Pearson's efficiency methods within ZEN 2009. The SPION-TRITC colocalization of lysosomes was calculated by coefficient $c_{SPION} = (Pixel_{colocalized}/Pixel_{total}) \times 100$. Likewise, the LysoTracker-labeled lysosomes were counted by coefficient $c_{lysosome} = (Pixel_{colocalized}/Pixel_{total}) \times 100$. The coefficient is reported as a percentage from 0 to 100, with 0 meaning no colocalization and 100 meaning all pixel-pairs are colocalized. Since TRITC labeled SPIONs were loaded into all the INS-1 cells after DMF treatment, we used the fluorescence intensity of TRITC to indicate the amount of SPIONs in a cell after 3 times washing. The total SPION loading efficiency was calculated by percentage of number of fluorescence intensity of TRITC to the intensity of Hoechst 34580 which reflects cell number in a field.

Transmission Electron Microscopy (TEM) Imaging. The preparation of cells for TEM was described previously.[42] Briefly, INS-1 insulinoma tumor cells[43] were treated with DMF, followed by fixation in 2.5% glutaraldehyde for 1 h at 4 °C. The cells were then treated with 1% osmium tetroxide, dehydrated, and embedded in AGAR100 (Oxford Instruments Nordiska AB, Stockholm) before they were sliced in ultrathin sections (70−90 nm). After slicing, the samples were placed on Cu grids and contrasted with uranyl acetate and lead citrate. The TEM images were obtained using a JEM 1230 electron microscope (Jeol-USA, Peabody, MA).

Human Islet Cell Immunostaining. Human islets were provided by the EXODIAB Human Tissue Lab and the Nordic Network of Clinical Islet Transplantation Programme (www.nordicislets.org). The islet cells were separated in a Ca^{2+}-free solution at 37 °C for 10 min and treated with DMF after 12 h culture on the coverslips centered dish (MatTek, Germany). Then, the cells were fixed with 3% PFA-PIPES and 3% PFA-Na_2BO_4 for 5 and 10 min, respectively, permeabilized with 0.1% Triton-X 100 for 30 min, and blocked with 5% normal donkey serum in PBS for 15 min. Guinea pig sourced antibody against insulin (EuroProxima, The

Netherlands) was diluted in 5% block buffer and incubated overnight at 4 °C. Immunoreactivity was done using fluorescently labeled secondary antibodies: cy2 anti-guinea pig (1:400) and cy5 anti-mouse (1:400). The images of SPION-TRITC (EX: 543 nm), cy2-labeled insulin (EX: 488 nm) and cy5-labeled LAMP1 (EX: 633 nm) were visualized through three or four channels by a confocal system (Zeiss, Germany). Lysosomal size (LAMP1 marked) was calculated using the profile function of the ZEN 2009 software based on the shapes of the fluorescence areas.

Intracellular pH Measurement. INS-1 cells were seeded on the glass centered dish (MatTek, Germany), loaded with SPION or SPION-LAMP1 and treated by DMF. Then, the cells were incubated with 1 μM acidic indicator, LysoSensor Green DND 189 (Invitrogen) for 30 min in 37 °C. After incubation, the cells were washed and the fluorescence images were acquired by confocal microscopy. The average fluorescence intensity per cell was measured using the ZEN 2009 software and further applied for quantitative analysis.

Cell Apoptosis Detection. FITC-Annexin V (51-65874X, BD) and 7-AAD (51-68981E, BD) were used to assess early and late apoptosis of INS-1 cells. After DMF treatment, the INS-1 cells were incubated with the dyes at 37 °C for 30 min. Images were acquired under identical conditions (using the same settings for pinhole (1 airy unit), exposure time, gain and scanning speed). Fluorescence intensity was analyzed by the ZEN 2009 software and early/late stage apoptosis was quantified by percentage of number of Annexin V/7-AAD positive cells to the number of Hoechst 34580 stained cells.

Proliferation. INS-1 cells were seeded on 24-well plates loaded with SPION or SPION-LAMP1 nanoparticles and treated by DMF once/day. Then, the cell number was calculated by a plate cytometer after 6 h of DMF treatment. Cells were counted once per day for 5 days.

Temperature Measurements. A dish with 100 nm SPIONs (10 mg/mL) in water and a dish without the SPIONs in water as a control, each containing a temperature sensor (Radial leaded glass-encapsulated NTC thermistor, EPCOS, Inc., Germany), were placed simultaneously on the DMF device. The dishes were then subjected to the DMF field for 20 min at 20 Hz and the temperature was recorded in each dish.

Statistical Analysis. The data was presented as average $\pm$ standard error of the mean (SEM). Statistical comparison of paired-factors experiments was performed by Student's *t* test and one-way analysis of variance (ANOVA), and the Friedman tests were performed for multifactor experiments, which have more than two group treatments in one experiment.

Conflict of Interest: The authors declare no competing financial interest.

Acknowledgment. The authors would like to thank Dipl.-Ing. Ernst Stetter for front-line technology development necessary for the project, Britt-Marie Nilsson and Anna Veljanovska Ramsay for expert technical assistance. This study was funded in part by project grants from the Swedish Research Council (E.R. and L.E.); the NovoNordisk Foundation (E.R.); and Region Skåne/Lund University (ALF; E.R. and L.E.); NIH K08 CA16396 (M.F.K.); RSNA Research Resident and Scholar grants (RR0824, 2380) (M.F.K.); an MSKCC Center for Molecular Imaging and Nanotechnology Center grant (M.F.K.); an MSKCC Technology Development Grant (M.F.K.) and The Dana Foundation (M.F.K.). M.F.K. is a 'Damon Runyon-Racleff Innovator'. The project has utilized infrastructure financed by the Linnaeus grant to Lund University Diabetes Center and the strategic research area in diabetes Exodiab. Human islets were obtained *via* the Exodiab Human Tissue Laboratory.

Supporting Information Available: Movie 1: illustrates the rotational control of magnetic micoparticles achieved with the DMF device. Movie 2: illustrates the rotational control of magnetic nanoparticles (300 nm diameter) achieved with the DMF device. Movie 3: dynamic confocal microscopy study of a single live cell illustrating injury to lysosomes *via* DMF and LAMP1-SPIONs in real-time. This material is available free of charge *via* the Internet at http://pubs.acs.org.

REFERENCES AND NOTES

1. Gaster, R. S.; Hall, D. A.; Nielsen, C. H.; Osterfeld, S. J.; Yu, H.; Mach, K. E.; Wilson, R. J.; Murmann, B.; Liao, J. C.; Gambhir, S. S.; *et al.* Matrix-Insensitive Protein Assays Push the Limits of Biosensors in Medicine. *Nat. Med.* **2009**, *15*, 1327–1332.
2. Haun, J. B.; Yoon, T. J.; Lee, H.; Weissleder, R. Magnetic Nanoparticle Biosensors. *Wiley Interdiscip. Rev.: Nanomed. Nanobiotechnol.* **2010**, *2*, 291–304.
3. Haun, J. B.; Castro, C. M.; Wang, R.; Peterson, V. M.; Marinelli, B. S.; Lee, H.; Weissleder, R. Micro-Nmr for Rapid Molecular Analysis of Human Tumor Samples. *Sci. Transl. Med.* **2011**, *3*, 71ra16.
4. Haun, J. B.; Devaraj, N. K.; Marinelli, B. S.; Lee, H.; Weissleder, R. Probing Intracellular Biomarkers and Mediators of Cell Activation Using Nanosensors and Bioorthogonal Chemistry. *ACS Nano* **2011**, *5*, 3204–3213.
5. Kircher, M. F.; Gambhir, S. S.; Grimm, J. Noninvasive Cell-Tracking Methods. *Nat. Rev. Clin. Oncol.* **2011**, 677–688.
6. Kircher, M. F.; Mahmood, U.; King, R. S.; Weissleder, R.; Josephson, L. A Multimodal Nanoparticle for Preoperative Magnetic Resonance Imaging and Intraoperative Optical Brain Tumor Delineation. *Cancer Res.* **2003**, *63*, 8122–8125.
7. Kircher, M. F.; Willmann, J. K. Molecular Body Imaging: MR Imaging, CT, and US. Part II. Applications. *Radiology* **2012**, *264*, 349–368.
8. Kircher, M. F.; Willmann, J. K. Molecular Body Imaging: MR Imaging, CT, and US. Part I. Principles. *Radiology* **2012**, *263*, 633–643.
9. Grimm, J.; Kircher, M. F.; Weissleder, R. [Cell Tracking. Principles and Applications]. *Radiologe* **2007**, *47*, 25–33.
10. Kozissnik, B.; Bohorquez, A. C.; Dobson, J.; Rinaldi, C. Magnetic Fluid Hyperthermia: Advances, Challenges, and Opportunity. *Int. J. Hyperthermia* **2013**, *29*, 706–714.
11. Laurent, S.; Dutz, S.; Hafeli, U. O.; Mahmoudi, M. Magnetic Fluid Hyperthermia: Focus on Superparamagnetic Iron Oxide Nanoparticles. *Adv. Colloid Interface Sci.* **2011**, *166*, 8–23.
12. Guo, M.; Que, C.; Wang, C.; Liu, X.; Yan, H.; Liu, K. Multifunctional Superparamagnetic Nanocarriers with Folate-Mediated and Ph-Responsive Targeting Properties for Anticancer Drug Delivery. *Biomaterials* **2011**, *32*, 185–194.
13. Wahajuddin; Arora, S. Superparamagnetic Iron Oxide Nanoparticles: Magnetic Nanoplatforms as Drug Carriers. *Int. J. Nanomed.* **2012**, *7*, 3445–3471.
14. Creixell, M.; Bohorquez, A. C.; Torres-Lugo, M.; Rinaldi, C. Egfr-Targeted Magnetic Nanoparticle Heaters Kill Cancer Cells without a Perceptible Temperature Rise. *ACS Nano* **2011**, *5*, 7124–7129.
15. Domenech, M.; Marrero-Berrios, I.; Torres-Lugo, M.; Rinaldi, C. Lysosomal Membrane Permeabilization by Targeted Magnetic Nanoparticles in Alternating Magnetic Fields. *ACS Nano* **2013**, *7*, 5091–5101.
16. Dobson, J. Remote Control of Cellular Behaviour with Magnetic Nanoparticles. *Nat. Nanotechnol.* **2008**, *3*, 139–143.
17. Corchero, J.; Villaverde, A. Biomedical Applications of Distally Controlled Magnetic Nanoparticles. *Trends Biotechnol.* **2009**, *27*, 468–476.
18. Kumar, C. S.; Mohammad, F. Magnetic Nanomaterials for Hyperthermia-Based Therapy and Controlled Drug Delivery. *Adv. Drug Delivery Rev.* **2011**, *63*, 789–808.
19. Wust, P.; Hildebrandt, B.; Sreenivasa, G.; Rau, B.; Gellermann, J.; Riess, H.; Felix, R.; Schlag, P. M. Hyperthermia in Combined Treatment of Cancer. *Lancet Oncol.* **2002**, *3*, 487–497.
20. Lee, J. H.; Jang, J. T.; Choi, J. S.; Moon, S. H.; Noh, S. H.; Kim, J. W.; Kim, J. G.; Kim, I. S.; Park, K. I.; Cheon, J. Exchange-Coupled Magnetic Nanoparticles for Efficient Heat Induction. *Nat. Nanotechnol.* **2011**, *6*, 418–422.
21. Ahmed, M.; Brace, C. L.; Lee, F. T., Jr.; Goldberg, S. N. Principles of and Advances in Percutaneous Ablation. *Radiology* **2011**, *258*, 351–369.
22. Gruttner, C.; Muller, K.; Teller, J.; Westphal, F.; Foreman, A.; Ivkov, R. Synthesis and Antibody Conjugation of Magnetic Nanoparticles with Improved Specific Power Absorption Rates for Alternating Magnetic Field Cancer Therapy. *J. Magn. Magn. Mater.* **2007**, *311*, 181–186.

23. El-Dakdouki, M. H.; Zhu, D. C.; El-Boubbou, K.; Kamat, M.; Chen, J. J.; Li, W.; Huang, X. F. Development of Multifunctional Hyaluronan-Coated Nanoparticles for Imaging and Drug Delivery to Cancer Cells. *Biomacromolecules* **2012**, *13*, 1144–1151.
24. Xu, H. F.; Dai, W.; Han, Y. H.; Hao, W.; Xiong, F.; Zhang, Y.; Cao, J. M. Differential Internalization of Superparamagnetic Iron Oxide Nanoparticles in Different Types of Cells. *J. Nanosci. Nanotechnol.* **2010**, *10*, 7406–7410.
25. Martin, A. L.; Hickey, J. L.; Ablack, A. L.; Lewis, J. D.; Luyt, L. G.; Gillies, E. R. Synthesis of Bombesin-Functionalized Iron Oxide Nanoparticles and Their Specific Uptake in Prostate Cancer Cells. *J. Nanopart. Res.* **2010**, *12*, 1599–1608.
26. Eto, K.; Yamashita, T.; Hirose, K.; Tsubamoto, Y.; Ainscow, E. K.; Rutter, G. A.; Kimura, S.; Noda, M.; Iino, M.; Kadowaki, T. Glucose Metabolism and Glutamate Analog Acutely Alkalinize Ph of Insulin Secretory Vesicles of Pancreatic Beta-Cells. *Am. J. Physiol. Endocrinol. Metab.* **2003**, *285*, E262–E271.
27. Cirman, T.; Oresic, K.; Mazovec, G. D.; Turk, V.; Reed, J. C.; Myers, R. M.; Salvesen, G. S.; Turk, B. Selective Disruption of Lysosomes in Hela Cells Triggers Apoptosis Mediated by Cleavage of Bid by Multiple Papain-like Lysosomal Cathepsins. *J. Biol. Chem.* **2004**, *279*, 3578–3587.
28. Mannix, R. J.; Kumar, S.; Cassiola, F.; Montoya-Zavala, M.; Feinstein, E.; Prentiss, M.; Ingber, D. E. Nanomagnetic Actuation of Receptor-Mediated Signal Transduction. *Nat. Nanotechnol.* **2008**, *3*, 36–40.
29. Cho, M. H.; Lee, E. J.; Son, M.; Lee, J. H.; Yoo, D.; Kim, J. W.; Park, S. W.; Shin, J. S.; Cheon, J. A Magnetic Switch for the Control of Cell Death Signalling in *in Vitro* and *in Vivo* Systems. *Nat. Mater.* **2012**, *11*, 1038–1043.
30. Tseng, P.; Judy, J. W.; Di Carlo, D. Magnetic Nanoparticle-Mediated Massively Parallel Mechanical Modulation of Single-Cell Behavior. *Nat. Methods* **2012**, *9*, 1113–1119.
31. Ivkov, R.; DeNardo, S. J.; Daum, W.; Foreman, A. R.; Goldstein, R. C.; Nemkov, V. S.; DeNardo, G. L. Application of High Amplitude Alternating Magnetic Fields for Heat Induction of Nanoparticles Localized in Cancer. *Clin. Cancer Res.* **2005**, *11*, 7093s–7103s.
32. Huang, H.; Delikanli, S.; Zeng, H.; Ferkey, D. M.; Pralle, A. Remote Control of Ion Channels and Neurons through Magnetic-Field Heating of Nanoparticles. *Nat. Nanotechnol.* **2010**, *5*, 602–606.
33. Burckhardt, C. J.; Greber, U. F. Virus Movements on the Plasma Membrane Support Infection and Transmission between Cells. *PLoS Pathog.* **2009**, *5*, e1000621.
34. Tomasini, M. D.; Rinaldi, C.; Tomassone, M. S. Molecular Dynamics Simulations of Rupture in Lipid Bilayers. *Exp. Biol. Med. (Maywood, NJ, U.S.)* **2010**, *235*, 181–188.
35. Ghosh, D.; Lee, Y.; Thomas, S.; Kohli, A. G.; Yun, D. S.; Belcher, A. M.; Kelly, K. A. M13-Templated Magnetic Nanoparticles for Targeted *in Vivo* Imaging of Prostate Cancer. *Nat. Nanotechnol.* **2012**, *7*, 677–682.
36. Gupta, A. K.; Gupta, M. Cytotoxicity Suppression and Cellular Uptake Enhancement of Surface Modified Magnetic Nanoparticles. *Biomaterials* **2005**, *26*, 1565–1573.
37. Bogart, L. K.; Taylor, A.; Cesbron, Y.; Murray, P.; Levy, R. Photothermal Microscopy of the Core of Dextran-Coated Iron Oxide Nanoparticles During Cell Uptake. *ACS Nano* **2012**, *6*, 5961–5971.
38. Schulze, K.; Koch, A.; Petri-Fink, A.; Steitz, B.; Kamau, S.; Hottiger, M.; Hilbe, M.; Vaughan, L.; Hofmann, M.; Hofmann, H.; *et al.* Uptake and Biocompatibility of Functionalized Poly(Vinylalcohol) Coated Superparamagnetic Maghemite Nanoparticles by Synoviocytes *in Vitro*. *J. Nanosci. Nanotechnol.* **2006**, *6*, 2829–2840.
39. Amstad, E.; Kohlbrecher, J.; Muller, E.; Schweizer, T.; Textor, M.; Reimhult, E. Triggered Release from Liposomes through Magnetic Actuation of Iron Oxide Nanoparticle Containing Membranes. *Nano Lett.* **2011**, *11*, 1664–1670.
40. Daniel, W. A.; Wojcikowski, J. Lysosomal Trapping as an Important Mechanism Involved in the Cellular Distribution of Perazine and in Pharmacokinetic Interaction with Antidepressants. *Eur. Neuropsychopharmacol.* **1999**, *9*, 483–491.
41. Kornhuber, J.; Henkel, A. W.; Groemer, T. W.; Stadtler, S.; Welzel, O.; Tripal, P.; Rotter, A.; Bleich, S.; Trapp, S. Lipophilic Cationic Drugs Increase the Permeability of Lysosomal Membranes in a Cell Culture System. *J. Cell. Physiol.* **2010**, *224*, 152–164.
42. Vikman, J.; Jimenez-Feltstrom, J.; Nyman, P.; Thelin, J.; Eliasson, L. Insulin Secretion Is Highly Sensitive to Desorption of Plasma Membrane Cholesterol. *FASEB J.* **2009**, *23*, 58–67.
43. Asfari, M.; Janjic, D.; Meda, P.; Li, G.; Halban, P. A.; Wollheim, C. B. Establishment of 2-Mercaptoethanol-Dependent Differentiated Insulin-Secreting Cell Lines. *Endocrinology* **1992**, *130*, 167–178.